Power-Based RFI Localization Using a Network of Unmodified COTS GNSS Receivers

Argyris Kriezis, *Stanford University*
Juan Blanch, *Stanford University*
Yu-Hsuan Chen, *Stanford University*
Dennis Akos, *University of Colorado Boulder*
Sherman Lo, *Stanford University*
Todd Walter, *Stanford University*

BIOGRAPHY

Argyris Kriezis is a PhD candidate in the Aeronautics and Astronautics program at Stanford University and part of the Stanford GPS Lab. He hold a BSc from Olin College of Engineering and a MS from Stanford University.

Juan Blanch is a senior research engineer at Stanford University. He holds an M.S. in electrical engineering from Ecole Polytechnique in France and a Ph.D. in aeronautics and astronautics from Stanford University.

Yu-Hsuan Chen is a research engineer at the Stanford GPS Laboratory. He received his Ph.D. in Electrical Engineering from National Cheng Kung University in 2011, Taiwan.

Dennis Akos completed the Ph.D. degree in Electrical Engineering at Ohio University in the Avionics Engineering Center with a focus on GPS/GNSS radio design and signal processing. Since 2005 he has been on the faculty with the Aerospace Engineering Science Department at University of Colorado at Boulder with a visiting appointment at the GPS Laboratory at Stanford University.

Sherman Lo is a senior research engineer at the Stanford GPS Laboratory. He received his Ph.D. in Aeronautics and Astronautics from Stanford University in 2002. He works on navigation robustness and safety, often supporting the FAA. He has conducted research on Loran, alternative navigation, SBAS, ARAIM, GNSS for railways and automobile. He also works on spoof and interference mitigation for navigation. He has published over 100 research papers and articles.

Todd Walter received his Ph.D. in Applied Physics from Stanford University in 1993. He is a Research Professor in the Department of Aeronautics and Astronautics at Stanford University. His research focuses on implementing high-integrity air navigation systems. He has received the ION Thurlow and Kepler awards. He is also a fellow of the ION and has served as its president.

ABSTRACT

The rising incidence of Radio Frequency Interference (RFI) affecting the Global Navigation Satellite System (GNSS) presents a significant risk to civilian, safety-critical infrastructure. While prior studies have shown that low-cost Commercial Off-The-Shelf (COTS) GNSS receivers can reliably detect interference, scalable low-cost methods for localizing RFI sources remain limited. This paper presents a power-based localization framework that enables networks of unmodified COTS GNSS receivers to progress from detection to source localization.

The proposed approach is based on a Power Difference of Arrival (PDOA) formulation, in which relative received power measurements across a distributed receiver network are used to infer the probable location of an emitter with unknown transmit power. A grid-based maximum likelihood algorithm is developed, incorporating a hardware-specific error model, chi-squared consistency testing, and an iterative receiver rejection process to improve robustness under non-ideal deployment conditions. To better reflect real-world environments, topographic data are integrated to refine slant-range calculations and antenna gain compensation.

The proposed method is developed using data from the 2024 Norway Jammer Test and validated with an independent dataset from the 2025 Norway Jammer Tests. The evaluated scenarios encompass jamming, meaconing, and spoofing events under non-ideal receiver network geometries. The results demonstrate that the system consistently estimates the true RFI source location within the derived predicted region, indicating that networks of low-cost GNSS receivers can provide a scalable and practical solution for RFI localization.

I. INTRODUCTION

The proliferation of Radio Frequency Interference (RFI) events targeting the Global Navigation Satellite System (GNSS) has exposed a critical global vulnerability. As society becomes increasingly reliant on precise positioning and timing data, the disruption of these signals poses significant risks to both safety and economic stability. Recent geopolitical conflicts in Eastern Europe and the Middle East have further demonstrated that RFI is no longer just a tactical military tool, but a persistent threat to civilian (Felux et al., 2024). To maintain operational continuity, civilian GNSS users must be able to detect, characterize, and localize RFI sources through cost-effective and scalable means.

Current RFI monitoring relies on a range of technologies, each with inherent trade-offs. Global methods, such as satellite-based monitoring reference and the analysis of Automatic Dependent Surveillance-Broadcast (ADS-B) data reference, offer a broad view of interference "hot spots." However, they often lack the detail required for local-scale insights. While satellite based monitoring can achieve high precision, its utility is constrained by high deployment costs and limited revisit rates. Conversely, ADS-B data provides a lower-cost alternative but suffers from poor spatial resolution, particularly in regions with sparse commercial air traffic.

In previous research, we demonstrated that carefully calibrated, affordable Commercial Off-The-Shelf (COTS) GNSS receivers are capable of robust RFI detection (Kriezis et al., 2025). This paper extends that work, presenting how a network of the same COTS receivers can move beyond detection to perform source localization. While existing localization systems often require multiple directional antennas, the algorithm presented here utilizes unmodified receivers (Madrid Cobos, 2021). This approach enables the development of high-density RFI moniotring networks that can be easily be deployed, providing the necessary RFI awareness to protect critical infrastructure, such as airports and maritime ports, in a scalable manner.

The proposed approach is based on the Power Difference of Arrival (PDOA) principle. Historically, PDOA has been successfully leveraged in terrestrial cellular networks, where the Received Signal Strength Indicator (RSSI) from multiple base stations is used to estimate a mobile handset's location with high precision (Vaghefi et al., 2013). However, a fundamental distinction exists between cellular localization and GNSS RFI characterization, the uncooperative nature of the source. In cellular environments, the network typically possesses knowledge of the target's transmit power or can command power control. In contrast, RFI localization must treat the transmit power (P_{tx}) as an additional unknown variable, forcing the network to rely solely on the relative power levels recorded at the sensing nodes (Xu et al., 2014).

In GNSS RFI localization, previous implementations of PDOA have generally followed two paths. The first involves utilizing the Automatic Gain Control (AGC) levels of GNSS receivers as a proxy for received power or signal C/N_0 values, typically under ideal geometry where the source is well positioned within the network (Blay and Akos, 2018; Borio et al., 2016). The second approach involves analyzing signal range over large geographic areas, focusing primarily on regions where the interference is strong enough for a receiver to lose signal lock (Tucker et al., 2020). This work advances these concepts by demonstrating that an RFI source can be bounded even under non-ideal deployment conditions, specifically, in scenarios where the receiver network geometry is suboptimal or the RFI source is situated outside the sensing network.

In this paper, the network model is first introduced in Section II, including the propagation model, topographic integration and the hardware-specific error modeling. The localization methodology is then discussed in Section III, outlining the grid-search algorithm, the iterative outlier rejection process, and the definition of probabilistic search regions. Finally, Section IV presents the experimental results and performance evaluation using the 2025 Norway Jammertest datasets.

II. NETWORK MODEL

GNSS receivers provide a range of observables that can be exploited for Radio Frequency Interference (RFI) detection and characterization. Building on prior work demonstrating that receiver-provided spectral information can be used to estimate RF power density, this paper leverages power-density measurements from a network of stationary receivers to localize RFI (Kriezis et al., 2025).

1. Propagation Model

The localization algorithm is based on the Free-Space Path Loss (FSPL) model, which characterizes signal attenuation between the interference source and each monitoring node. In a typical localization scenario, the source coordinates constitute the unknown parameters to be estimated. Given a network of N receivers at known locations, the source position can be inferred by analyzing the relative power differences observed across the network.

However, transitioning this from theory to a real-world environment introduces two primary challenges. First, the standard FSPL model does not account for terrestrial complexities such as multi-path fading, shadowing, or physical obstructions like buildings and terrain. Second, the network geometry, dictated by the spatial distribution of the receivers relative to the source significantly impacts the final estimation accuracy.

To model the signal path from the RFI source to the receiver's input port, several variables must be considered. Because the transmit power (P_t) and the transmit antenna gain (G_t) of an interference source are unknown, they are grouped into a single Equivalent Isotropic Radiated Power (EIRP) variable. Grouping the transmit power and gain into a single variable assumes that either the antenna is unidirectional or the monitoring receiver lie within the directional antenna's main lobe.

The received power at a given node i is presented in Equation 1.

$$P_{\mathrm{rx},i} = \mathrm{P}_{\mathrm{tx,eirp}} - L_{\mathrm{fspl},i} - L_{\mathrm{obs},i} + G_{\mathrm{rx},i} + \epsilon \tag{1}$$

The received power at a monitoring node is a complex function of several environmental and hardware factors. Specifically, $P_{\mathrm{rx},i}$ depends on the free-space path loss ($L_{\mathrm{fspl},i}$), potential signal attenuation due to physical obstructions ($L_{\mathrm{obs},i}$), the receiver's antenna gain ($G_{\mathrm{rx},i}$), and an error term (ϵ) representing unmodeled effects such as multipath. The path loss model is defined in Equation 2:

$$L_{\mathrm{fspl}} = n10\log_{10}\left(\frac{4\pi d}{\lambda}\right) \tag{2}$$

In this model, d_i represents the distance between the RFI source and the i-th receiver, λ is the signal wavelength, and n is the path loss exponent. While $n = 2$ characterizes ideal free-space conditions, this value typically ranges from 2 to 2.3 in terrestrial environments to account for partial blocking, shadowing and ground reflections (Dharmadhikari et al., 2018).

The obstruction loss term, $L_{\mathrm{obs},i}$, presents a significant challenge in estimating the received power. Although this parameter could theoretically be estimated through 3D mapping of the deployment area, such data is rarely available for real-time monitoring. Instead, the proposed model mitigates these uncertainties by utilizing the path loss exponent to aggregate the effects of partial obstructions, such as foliage or light urban structures. Furthermore, in cases where a receiver experiences a total signal blockage, non-line-of-sight (NLOS) condition, the resulting low-power reading can be removed from the localization through isolation. Consequently, the baseline model presented in this work integrates $L_{\mathrm{obs},i}$ into the path loss exponent terms.

The receiver antenna gain ($G_{\mathrm{rx},i}$) is treated as a known parameter, provided that the manufacturer supplies the antenna pattern data. While GNSS antennas typically offer a relatively uniform gain profile at high elevation angles, lower-elevations, where ground based emitters are typically located, often exhibit a different gain based on the signal angle of arrival. As a result. the received power changes based on the direction the signal is arriving from. By leveraging the provided antenna gain pattern, these directional fluctuations can be compensated for within the power model, assuming the angles of arrival can be estimated or approximated during the localization process.

2. Receiver Network

In a receiver network, the recorded power at each node is used to estimate the location of an interference source. For any candidate coordinate within a search grid, the expected received power is calculated via a propagation model and compared against the measured data. The residuals between theoretical and recorded values are minimized when the candidate location converges on the true RFI source. In a two-dimensional space, a minimum of three receivers is required to reach a unique solution when the transmit power of the RFI source is unknown. Figure 1 illustrates this network configuration over a discrete grid. For each grid cell, the system evaluates the likelihood of the source's presence by analyzing the correlation between the modeled and observed signal levels.

Equation 1 and Equation 2 are rearranged to solve for the equivalent isotropically radiated power ($P_{\mathrm{tx,eirp}}$) at a candidate location x, based on the power $P_{\mathrm{rx},i}$ recorded at the i-th receiver located at y_i. This relationship is defined in Equation 3.

$$\mathrm{P}_{\mathrm{tx,eirp}}(x, y_i) = P_{\mathrm{rx},i} + n10\log_{10}\left(\frac{4\pi d(x, y_i)}{\lambda}\right) - G_{\mathrm{rx},i}(x, y_i) \tag{3}$$

Equation 4 re-writes the same equation grouping the path loss and receiver gain in a single propagation function p with inputs the candidate location x and the receiver location y_i.

$$\mathrm{P}_{\mathrm{tx,eirp}}(x, y_i) = P_{\mathrm{rx},i} + p(x, y_i) \tag{4}$$

To evaluate the probability of each grid point being the true location of the RFI source, a log-likelihood method is employed. This approach operates on the assumption that the measurement error at each receiver is Gaussian with constant parameters regardless of the receiver's position in the network or its distance from the source. The log-likelihood is calculated as presented

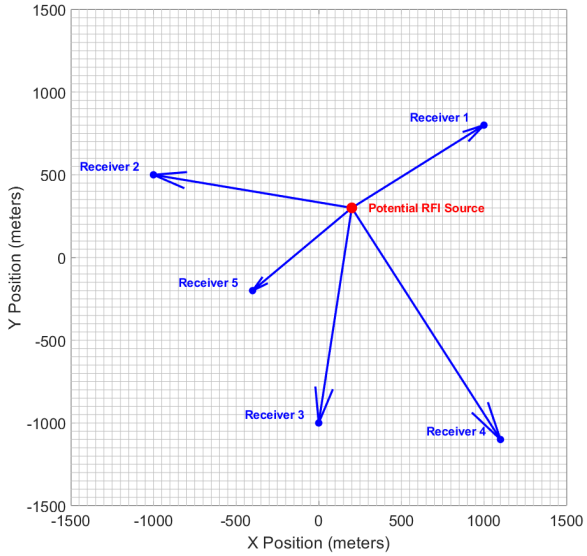

Figure 1: Example receiver network grid with the distances to a potential RFI source location

in Equations 5 and 6. While this error model assumes a uniform error distribution, a distance-varying error model can be implemented in the future.

$$\hat{P}_{tx,eirp}(x) = \frac{\sum_{i=1}^{N} \frac{P_{\mathrm{rx},i} + p(x,y_i)}{\sigma_i^2}}{\sum_{i=1}^{N} \frac{1}{\sigma_i^2}} \tag{5}$$

where σ_i is the Gaussian error of the i-th receiver.

$$\ell(x) = \frac{1}{2}\sum_{i=1}^{N} \log\left(2\pi\sigma_i^2\right) - \frac{1}{2}\sum_{i=1}^{N} \frac{\left(P_{\mathrm{rx},i} + p(x,y_i) - \hat{P}_{tx,eirp}(x)\right)^2}{\sigma_i^2} \tag{6}$$

The likelihood is evaluated for every grid point within the monitored area. Given that the free-space path loss exponent typically ranges between 2 and 2.3, the log-likelihood is iteratively calculated across this range. The exponent value that maximizes the likelihood is selected as the optimal parameter for each grid point. The resulting grid demonstrates the areas in the monitored area that are more likely to contain the RFI source.

While two-dimensional models provide a useful baseline, simplifying the real-world environment to a flat plane often yields inaccurate localization for RFI sources in complex terrain. To refine the model, NASA ASTER (Advanced Spaceborne Thermal Emission and Reflection Radiometer) data are integrated to provide precise topological information for the monitored area. This topographic integration offers two primary enhancements. First, it allows for a more accurate calculation of the slant-range distance between the emitter and receiver by accounting for altitude differentials. Second, and more critically, it enables the derivation of the signal angle of arrival, providing both azimuth and elevation data to determine the precise antenna gain pattern.

3. Error Modeling

Error modeling is fundamental in achieving an accurate representation of the RFI source location. Each component of the propagation model contributes to a cumulative measurement error, which directly dictates the precision and uncertainty bounds of the final estimation. While measurement error are quantified in decibels (dB), the source distance estimate is expressed in meters. Due to the exponential nature of path loss, the sensitivity of the distance estimate increases significantly with range. This error expansion is illustrated in Figure 2, which maps the distance error in meters relative to a range of measurement uncertainties. At a distance of 500 meters between the receiver and an RFI source, the error of a 0.5 dB measurement uncertainty is a little over 55 meters, while at 2 km about 230 meters. The same errors for a 1 dB measurement uncertainty are 115 and 462 meters.

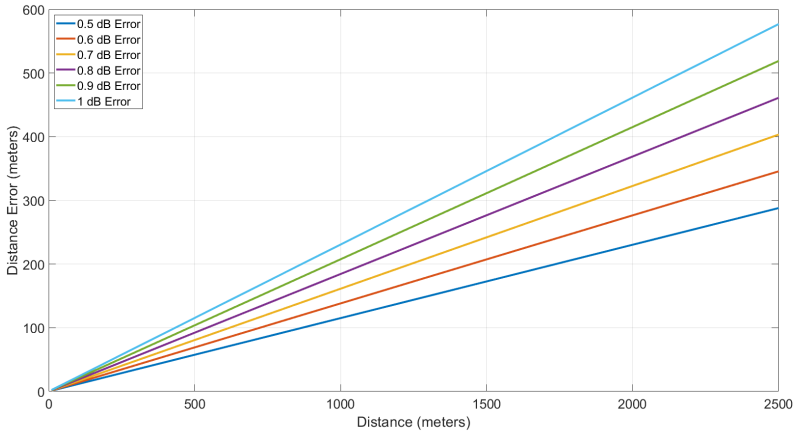

Figure 2: Estimated distance error in meters for 0.5 dB of measurement uncertainty over a range of distance between a source and a receiver

The first source of error stems from the intrinsic measurement accuracy of the receiver hardware. By analyzing the fluctuations in the received power metric under nominal, non-RFI conditions, the measurement uncertainty can be determined. For most receivers, this error adheres to a Gaussian distribution with a standard deviation (σ) typically ranging between 0.1 and $0.2\,dB$. However, this value is sensitive to deployment-specific factors, such as the integrity of antenna connections or hardware degradation. Consequently, the model incorporates real-time updates to the error parameters by continuously monitoring measurement oscillations. Figure 3 illustrates the Gaussian fit of the empirical measurement error for a representative receiver node.

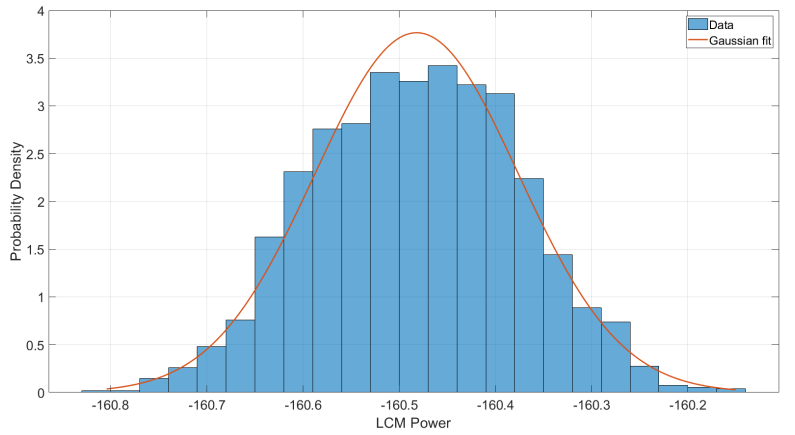

Figure 3: Estimated distance error in meters for 0.5 dB of measurement uncertainty over a range of distance between a source and a receiver

The second error source arises from the receiver's antenna gain pattern. By leveraging manufacturer-provided gain patterns, this error is characterized through two primary factors, azimuth and elevation accuracy. Topological data provides the geometric context necessary to calculate the 3D angle of arrival (AoA) between a candidate RFI source location and the receiver node. However, uncertainty regarding the physical orientation of the antenna introduces substantial measurement bias. Notably, at low elevation angles (below 15 degrees), the azimuth-dependent gain variance can exceed 3 dB, significantly impacting localization accuracy. To address this, the algorithm operates in two distinct modes: a 'Calibrated' mode where the antenna orientation is known, and an 'Uncalibrated' mode where orientation is unknown. In the latter case, the gain error σ is set higher to a range of 0.8 to 1.6 dB, depending on the specific antenna model utilized. For the systems with known antenna orientation, the gain error ranges 0.4-0.8dB to account for uncertainty in the orientation given the placement is subject to human error.

A third error term is included to account for remaining propagation uncertainties, such as multipath and partial obstruction. This term is more difficult to characterize because it depends on the local environment, however, based on the variance observed in interference measurements from RFI tests, a value of 0.25 dB is used.

The aggregate error of each receiver in the system is a combination of the hardware measurement uncertainty, antenna gain-related variances and propagation uncertainty. To maintain high estimation accuracy under changing conditions, the localization algorithm is designed to adapt these error parameters in real-time. By continuously monitoring measurement oscillations, the system can dynamically tune the error bound and similarly if a receiver's physical placement or orientation is modified, the algorithm adjusts the corresponding gain uncertainty. As established at the beginning of this subsection, the error model defines the variance of the residuals, which increases as a function of distance for a fixed power uncertainty. Consequently, higher uncertainty in the measured values directly correlates to a larger probable region in which the RFI source may be located.

III. LOCALIZATION METHODOLOGY AND ALGORITHM

The proposed network model serves as the foundation for a location estimation algorithm designed to bound the probable region of an RFI source. Utilizing a Power Difference of Arrival (PDOA) approach on cost-effective hardware, the system's objective is to provide critical situational awareness. Rather than aiming for centimeter-level geolocation, the model prioritizes the distinction between internal and external interference relative to a protected zone, when narrowing the RFI source search area. While higher precision is attainable via the use of directional antennas, this COTS receiver network provides a low-cost baseline that maintains operational utility under non-ideal geometries and at significant ranges.

1. Grid Search Methodology

The localization algorithm employs a grid search approach, discretizing the monitored area into cells with a radius of 10–50 meters, depending on user-defined resolution requirements. The receiver nodes are stationary, with fixed coordinates and altitudes. To improve the accuracy of the propagation model, topographic data (NASA ASTER) is integrated to account for altitude-dependent slant-range calculations.

Initial system deployment requires the calibration of all receiver nodes under nominal, RFI-free conditions. This process normalizes the noise floor across the hardware units to ensure measurement consistency. The error model is hardware-specific and highly dependent on the precision of the antenna's physical orientation. In scenarios where the orientation is unknown, the algorithm defaults to a gain model utilizing the mean antenna gain for a given elevation angle alongside an expanded error bound.

For each discrete epoch, updated at a 1 Hz frequency, the likelihood of each grid cell is calculated using the collective measurements of all available receivers. The likelihood of a candidate coordinate (x, y) being the true source location is derived from the convergence of the measured power values across all nodes, as seen in Equations 6. To ensure the integrity of the solution, a Chi-squared (χ^2) test is performed at the coordinate of maximum likelihood to evaluate the residuals between measured and modeled power values.

In the event that the fit fails the χ^2 threshold, the algorithm initiates a recursive receiver mitigation process. During this cycle, the receiver recording the lowest power value is excluded, and the likelihood and χ^2 test are recalculated. This iterative rejection continues until either the statistical test is satisfied or the network reaches a minimum of three receivers. These three nodes represent the mathematical minimum required to solve for the unknown 2D coordinates and the unknown transmit power ($P_{\text{tx,eirp}}$) of the source.

To provide actionable situational awareness to the end user, the likelihood values over the spatial grid are normalized to define a probable source region. This region is constructed by aggregating grid cells until a predefined cumulative probability threshold, such as 90%, is reached. The choice of this threshold reflects a fundamental trade-off between confidence and spatial precision: higher probability thresholds increase the likelihood of containing the true source location but result in a broader spatial extent, whereas lower thresholds produce a more compact region at the expense of an increased risk of excluding the true emitter. The spatial extent of the probable region is further influenced by the sensitivity of the underlying error model (σ), with larger measurement uncertainties leading to an expansion of the region's area.

The system operates as a 2D-surface model, while it incorporates 3D topographic altitude for distance calculations, the search space is constrained to the ground plane. Consequently, the system is designed for stationary and mobile ground-based transmitters and does not currently estimate the altitude of airborne RFI sources. The model parameters were fine-tuned using the 2024 Jammertest data set (Norway), with a distinct data set from the 2025 Jammertest utilized for objective evaluation.

2. Example Implementation

To demonstrate the proposed algorithm, representative results from the 2024 Jammertest in Bleik, Norway, are analyzed. Two distinct scenarios are presented to evaluate the model's performance under varying geometric conditions, an RFI source located outside the receiver network perimeter and a source situated in close proximity to a single network node. In addition, the difference between a network with known and unknown antenna orientation is presented.

The receiver network consisted of five stationary nodes distributed throughout the town of as seen in Figure 4. The experiment reflects a realistic suburban environment, characterized by varying building heights, local vegetation, and complex signal-propagation paths. Unlike controlled laboratory setups or open-field tests, these receiver installations lacked unobstructed aerial views and purpose-built mounting structures, thereby introducing a higher degree of realism to the measurements.

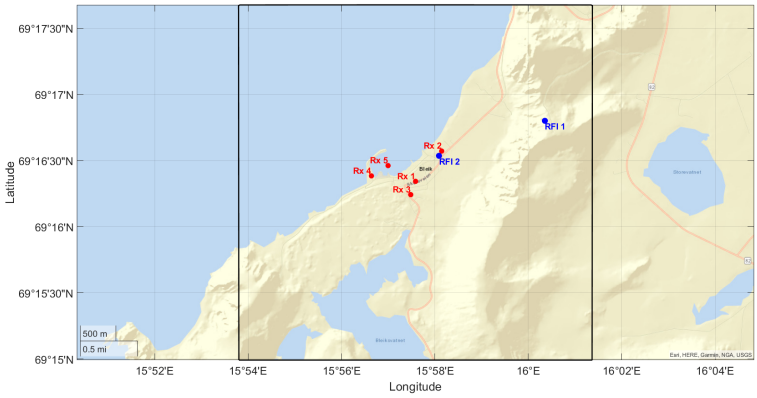

Figure 4: Jammer test 2024 receiver network setup relative to the two RFI sources

The primary output of the location estimation algorithm is a spatial probability density defined over the grid. Figure 5 illustrates three representative test scenarios sampled from the first three days of the 2024 Jammer Test (NPRA, 2024). Figure 5a corresponds to a receiver network with known antenna orientations and an RFI source located in mountainous terrain. Figure 5b shows the same source location using a network with unknown antenna orientations. Figure 5c presents a scenario with unknown antenna orientations and an RFI source located in town adjacent to receiver node 2.

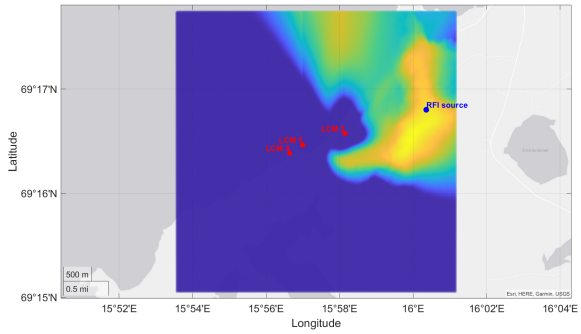

(a) RFI case 1: Known receiver orientation and source in the mountain

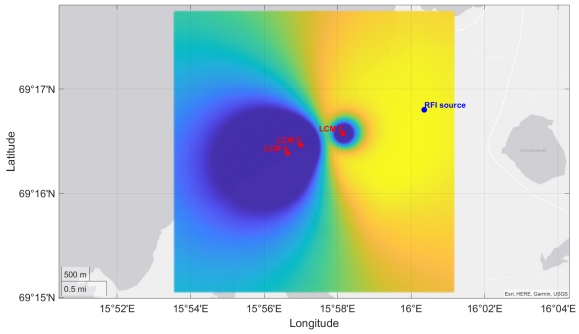

(b) RFI case 2: Unknown receiver orientation and source in the mountain

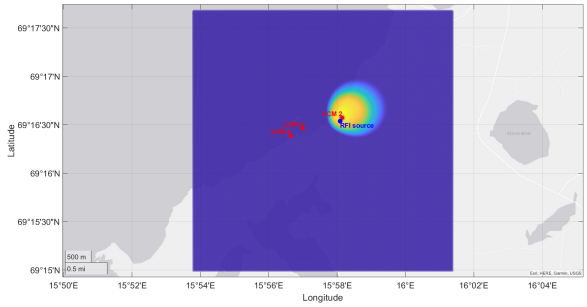

(c) RFI case 3: Unknown receiver orientation and source in the town

Figure 5: Localization grid probability density for three RFI cases

The probability density maps illustrate the impact of measurement uncertainty on the spatial dispersion of the likelihood across the grid. In the two scenarios where the RFI source is located in mountain, the high measurement uncertainty due to the long distance results in a broadly distributed probable region spanning a large portion of the search space. In contrast, when the source is located within the town, the probability mass is tightly clustered around the true emitter location. A direct comparison between networks with known and unknown antenna orientation further highlights the impact of measurement uncertainty. In the case with known antenna orientation, the resulting likelihood better represents the RFI source region compared to the uncalibrated configuration, which has an approximately circular bound.

The second output of the localization algorithm defines the probable RFI source location by aggregating the grid cells that constitute the top 90% of the cumulative probability (90% confidence). Figure 6 illustrates these probable regions for the three RFI cases, providing a spatial representation of the system's specificity under varying geometric and error conditions.

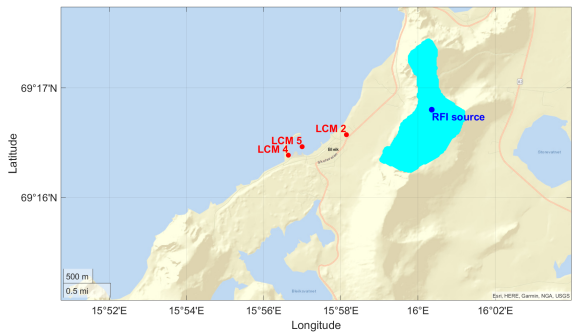

(a) RFI case 1: Known receiver orientation and source in the mountain

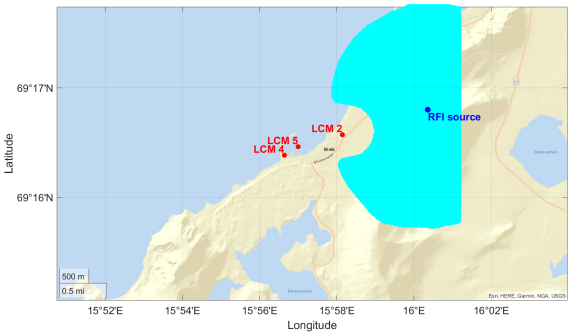

(b) RFI case 2: Unknown receiver orientation and source in the mountain

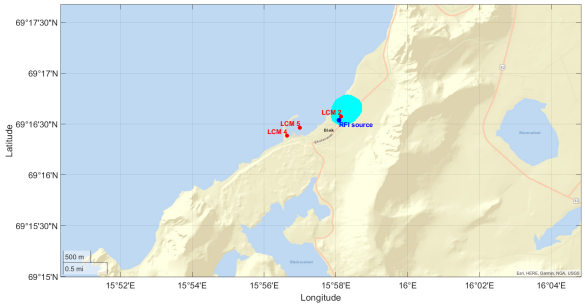

(c) RFI case 3: Unknown receiver orientation and source in the town

Figure 6: RFI source location estimation for three RFI cases (90% of probability)

While the 90% confidence threshold provides high confidence that the true source lies within the defined region, alternative thresholds can be applied to reduce the spatial extent of the probable area. Figure 7 illustrates the same three RFI scenarios with color-coded regions corresponding to 90%, 75%, and 50% probability levels, demonstrating the trade-off between confidence and spatial precision.

Although the specific epochs shown in Figure 7 capture the true RFI source locations within both the 90% and 75% probability bounds, this may not hold consistently over the full duration of a test. The 50% bound substantially reduces the extent of the localization region, however, even in the three illustrative cases presented, the true source falls outside the bound for case 1, highlighting the trade-off between localization resolution and confidence.

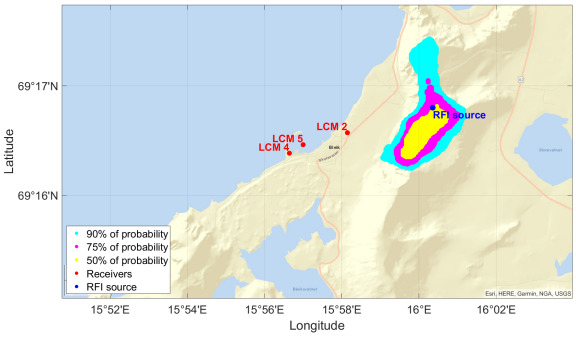

(a) RFI case 1: Known receiver orientation and source in the mountain

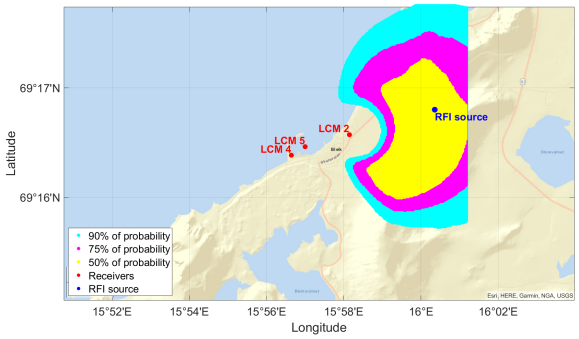

(b) RFI case 2: Unknown receiver orientation and source in the mountain

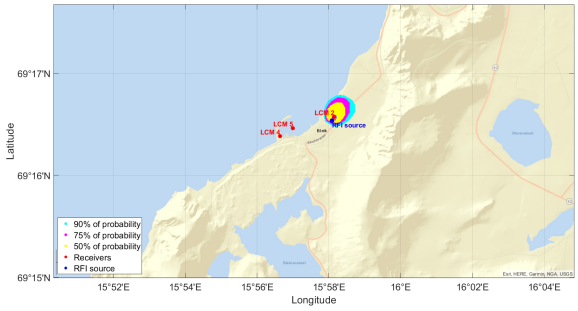

(c) RFI case 3: Unknown receiver orientation and source in the town

Figure 7: RFI source location estimation for three RFI cases at a range of grid space probabilities (50%, 75% and 90%)

IV. REAL WORLD EVALUATION

1. Network and Experiment Outline

The 2025 jammer test setup, used for validation of the algorithm, was similar to that of the previous year, with modifications to the geometry of the deployed receiver network. Figure 8 illustrates the locations of the RFI sources and receiver nodes used to validate the proposed location estimation algorithm. Although identical receiver hardware was used at all nodes, the antenna orientations were not known.

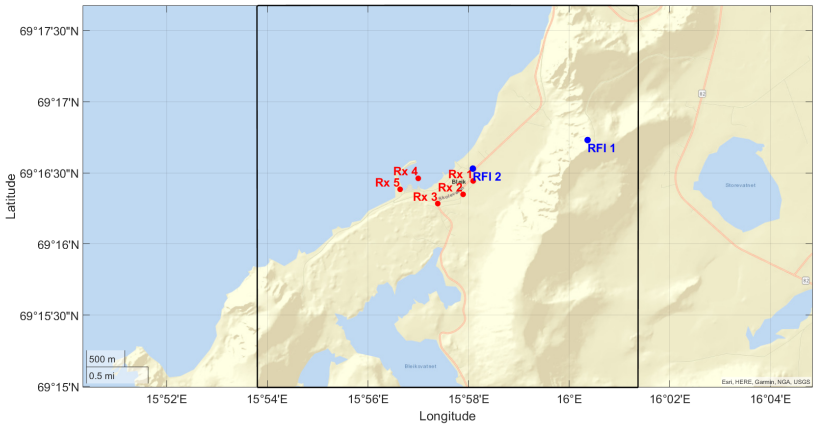

Figure 8: Jammer test 2025 receiver network setup relative to the two RFI sources

Table 1 summarizes the RFI events from the jammer test selected for algorithm evaluation. These events encompass multiple

interference types, including jamming, meaconing and spoofing. Additional details on the test campaign are available in the event's GitHub repository (NPRA, 2025). Importantly, the 2025 data were not used during the development of the localization algorithm and therefore serve as an independent data set for validation.

Table 1: Evaluation RFI Events

Test	Test Time	RFI Type	Location	Duration	Antenna Orientation
1	2025-09-15 14:50-15:00	50W Frequency Sweep L1	Mountain	10 minutes	unknown
2	2025-09-15 15:40-15:50	50W PRN L1 Jamming	Mountain	10 minutes	unknown
3	2025-09-15 16:05-16:15	50W PRN L1/G1 Jamming	Mountain	10 minutes	unknown
4	2025-09-16 10:20-10:30	Meaconing at 10 W	Mountain	10 minutes	unknown
5	2025-09-16 10:45-11:00	Jamming and Meaconing at 10 W	Mountain	15 minutes	unknown
6	2025-09-16 11:25-11:40	Meaconing with ramping power	Mountain	15 minutes	unknown
7	2025-09-17 10:40-10:55	GPS and Galileo Spoofing	Town	15 minutes	unknown
8	2025-09-17 11:25-11:40	Spoofing (Moving Location)	Town	15 minutes	unknown
9	2025-09-17 12:45-13:00	EGNOS Spoofing	Town	15 minutes	unknown

2. Results and Evaluation

Figure 9 presents the RFI source localization results for three different probability bounds. Of the nine tests used to validate the localization algorithm, representative results from Tests 3, 4, 8, and 9 are shown.

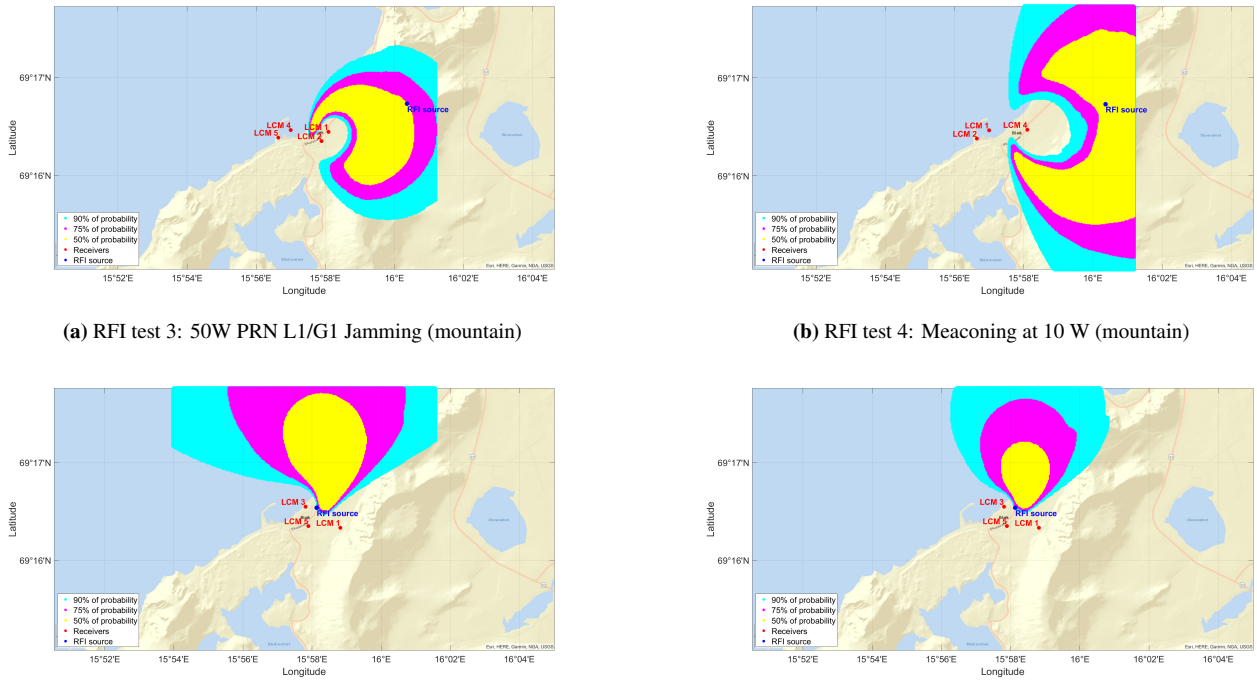

(a) RFI test 3: 50W PRN L1/G1 Jamming (mountain)

(b) RFI test 4: Meaconing at 10 W (mountain)

(c) RFI test 8: Spoofing - Moving Location (town)

(d) RFI test 9: EGNOS Spoofing (town)

Figure 9: RFI source location estimation for tests 3, 4, 8 and 9 at a range of probability bounds (50%, 75% and 90%)

The results for the six test scenarios listed in Table 1 are summarized in Table 2 for the confidence bounds of 50%, 75%, and 90%. Localization performance is assessed using two primary metrics: Accuracy, if the true RFI source is located within the probable region and the mean area of the probable region.

3. Discussion

The experimental results demonstrate that a network of Commercial Off-The-Shelf (COTS) GNSS receivers is capable of effectively localizing RFI sources across a range of jamming conditions, including scenarios with non-ideal network geometries.

Table 2: Localization Algorithm Performance Results

Test	Covered Region (90% Probability)			Covered Region (75% Probability)			Covered Region (50% Probability)		
	Accuracy	**Avg. Error**	**Avg. Area**	**Accuracy**	**Avg. Error**	**Avg. Area**	**Accuracy**	**Avg. Error**	**Avg. Area**
1	100%	0 m	9.39 km^2	100%	0 m	6.93 km^2	98.3%	0.5 m	4.09 km^2
2	100%	0 m	7.66 km^2	100%	0 m	5.29 km^2	100%	0 m	3.02 km^2
3	99.8%	0.5 m	5.95 km^2	99.4%	2.8 m	3.84 km^2	48.5%	46.5 m	2.01 km^2
4	100%	0 m	9.03 km^2	100%	0 m	6.61 km^2	95.9%	5.4 m	3.95 km^2
5	99.5%	5.0 m	7.18 km^2	94.8%	7.4 m	4.97 km^2	64.5%	115.5 m	2.85 km^2
6	98.8%	4.4 m	8.23 km^2	96.9%	15.6 m	5.87 km^2	78.6%	56.9 m	3.43 km^2
7	24.6%	15.0 m	8.11 km^2	8.1%	32.5 m	4.96 km^2	0.2%	59.3 m	2.24 km^2
8	66.3%	8.0 m	4.13 km^2	51.6%	17.1 m	2.19 km^2	0.0%	60.1 m	0.94 km^2
9	71.2%	7.8 m	5.02 km^2	0.5%	32.0 m	2.48 km^2	0.0%	78.8 m	0.79 km^2
Avg.	**84.5%**	**4.5 m**	**7.20 km^2**	**72.4%**	**11.9 m**	**4.79 km^2**	**54.0%**	**47.3 m**	**2.48 km^2**

With the exception of Test 7, the RFI source location was accurately estimated. In Test 7, while the accuracy is lower, the localization error is only a few meters off and can be attributed to unknown antenna orientation. These results highlight the critical role of the antenna gain pattern in the system accuracy.

In agreement with the proposed error model, measurement uncertainty increases with range, as evidenced by the expanded probable regions observed when the interference source was located in the mountain more than 1.5 km from the nearest receiver node. Despite the resulting increase in spatial extent, the system consistently located the emitter to the correct area, providing actionable intelligence that narrows the search region for mitigation efforts. Moreover, the use of selectable localization confidence level, enables a tunable trade-off between localization accuracy and spatial resolution, allowing users to choose an appropriate confidence level based on operational requirements.

Although the current error model imposes a fundamental limit on absolute localization precision, the spatial extent of the probable region can be reduced through improved hardware calibration, such as deploying receiver antennas with known orientations. In addition, while the inclusion of receiver isolation techniques enhances localization accuracy, further improvements remain possible. In particular, incorporating information about physical obstructions and explicitly modeling multipath propagation could further improve the robustness of the proposed power-based localization approach.

V. CONCLUSION

This paper demonstrates the feasibility of leveraging a network of low-cost, COTS GNSS receivers to progress beyond RFI detection towards reliable source localization. Using a PDOA framework, the proposed approach provides a scalable solution capable of delivering the RFI situational awareness required to protect critical infrastructure.

The integration of topographic data plays a key role in refining the propagation model, enabling the algorithm to account for altitude-dependent slant-range effects and variations in signal angles of arrival. In addition, the incorporation of a hardware-specific error model allows the system to account for receiver-dependent measurement uncertainties. Experimental results from the 2025 Norway Jammer Tests demonstrate that, even under suboptimal network geometry and unknown antenna orientations, the proposed method can effectively constrain the location of RFI sources. The use of an iterative measurement rejection strategy combined with χ^2 consistency testing further enhances robustness, particularly in the presence of Non-Line-of-Sight (NLOS) conditions and complex propagation environments.

In summary, this study confirms the viability of using networks of COTS GNSS receivers for RFI source localization. By eliminating reliance on expensive, systems with directional antennas, the proposed methodology offers a scalable and cost-effective solution for continuous interference monitoring at critical infrastructure sites. The experimental validation shows that meaningful spatial bounds on interference sources can be achieved even with limited hardware calibration and non-ideal geometry. Overall, the presented framework represents a practical pathway toward improving GNSS interference awareness.

ACKNOWLEDGEMENTS

We would like to acknowledge our industry and academic partners for hosting our GNSS receivers in their locations for the collection of the data for this paper. We would also like to acknowledge the support of The Aerospace Corporation under their University Partnership Program, the DOT's CARNATIONS center and the FAA for supporting this effort. The author also acknowledges the use of Large Language Models (LLM) for editing purposes.

REFERENCES

Blay, R. C. and Akos, D. M. (2018). Gnss rfi localization using a hybrid tdoa/pdoa approach. In *Proceedings of the 2018 International Technical Meeting of The Institute of Navigation*, pages 703–712, Reston, Virginia.

Borio, D., Gioia, C., Štern, A., Dimc, F., and Baldini, G. (2016). Jammer localization: From crowdsourcing to synthetic detection. In *Proceedings of the 29th International Technical Meeting of the Satellite Division of The Institute of Navigation (ION GNSS+ 2016)*, pages 3107–3116, Portland, Oregon.

Dharmadhikari, V., Pusalkar, N., and Ghare, P. (2018). Path loss exponent estimation for wireless sensor node positioning: Practical approach. In *2018 IEEE International Conference on Advanced Networks and Telecommunications Systems (ANTS)*, pages 1–4.

Felux, M., Fol, P., Figuet, B., Waltert, M., and Olive, X. (2024). Impacts of global navigation satellite system jamming on aviation. *NAVIGATION: Journal of the Institute of Navigation*, 71(3).

Kriezis, A., Chen, Y.-H., Akos, D., Lo, S., and Walter, T. (2025). Gnss jamming and spoofing monitoring using low-cost cots receivers. *Submitted to* NAVIGATION: Journal of the Institute of Navigation. Preprint on arXiv.

Madrid Cobos, J. (2021). Dylema-madrid: Madrid airport and tma gnss rfi monitoring system. Technical report, United Nations Office for Outer Space Affairs (UNOOSA), International Committee on GNSS (ICG), Virtual. Presentation/technical report.

NPRA (2024). Jammer test transmission plan. `https://github.com/NPRA/jammertest-plan/blob/5349470b4ecdaedc53360a9ae4958abb5a8325f8/Transmissionplan.pdf`.

NPRA (2025). Jammer test transmission plan. `https://github.com/NPRA/jammertest-plan`.

Tucker, J. A., Puskar, C., Lee, C., and Akos, D. (2020). Gps/gnss interference power difference of arrival (pdoa) localization weighted via nearest neighbors. In *Proceedings of the 33rd International Technical Meeting of the Satellite Division of The Institute of Navigation (ION GNSS+ 2020)*, pages 3550–3560.

Vaghefi, R. M., Gholami, M. R., Buehrer, R. M., and Strom, E. G. (2013). Cooperative received signal strength-based sensor localization with unknown transmit powers. *IEEE Transactions on Signal Processing*, 61(6):1389–1403.

Xu, Y., Zhou, J., and Zhang, P. (2014). Rss-based source localization when path-loss model parameters are unknown. *IEEE Communications Letters*, 18(6):1055–1058.